The influence of coral reef spur and groove morphology on wave energy dissipation and wave overtopping under future climate change scenarios

Lachlan Perris[1,*], Tristan Salles [1], Thomas E Fellowes[1], Stephanie Duce[2], Jody Webster[1], Ana Vila-Concejo[1]

[1] Geocoastal Research Group and Marine Studies Institute, School of Geosciences, The University of Sydney, NSW, 2006, Australia

[2] College of Science and Engineering, James Cook University, Bebegu Yumba Campus, Townsville, Queensland 4811, Australia

* Corresponding Author, lachlan.perris@sydney.edu.au

Key Points:

- Accurate bathymetries (<1 m) in forereef wave energy dissipation models highlight previously overlooked features of the forereef, including spurs and grooves (SaG).
- SaG influence forereef wave energy dissipation and this influence can be related to the SaG morphology.
- Future climate change projections modify dissipation rates by shifting the dominant mode of dissipation (from bed friction to wave breaking) leading to an increase wave overtopping on forereefs.

Abstract

Coral reefs protect coastlines from inundation and flooding, servicing over 200 million people globally. Wave transformation has previously been studied on coral reef flats with limited focus on forereef zones where wave transformation is greatest during high-energy conditions. This study investigates the role of forereef spur and groove (SaG) morphology on wave energy dissipation and overtopping on coral reefs. Using XBeach on LiDAR-derived bathymetry, we reproduced dissipation rates comparable to SaG field studies under present-day conditions. Our results highlight the benefits of accurate bathymetries in forereef wave energy dissipation models, as they incorporate critical morphological features (e.g., groove sinuosity, irregular forereef slopes) that exert control over mode of wave energy dissipation (frictional and breaking). We then investigated changes to wave energy dissipation and wave overtopping based on IPCC AR5 low and high emission scenarios

(RCP2.6 and RCP8.5) and a total disaster scenario (TD) for the year 2100 considering changes to SaG morphology, wave power and relative sea-level rise. For RCP2.6, an increase in wave heights of 0.8 m and an increase in water level of 0.3 m resulted in a two-fold increase in dissipation rates. For RCP8.5 and TD, with no increase in incident wave height, dissipation rates were 29% and 395% lower than RCP2.6. This resulted in increased overtopping at the reef crest by 1.8 m and 2.7 m for RCP8.5 and TD scenarios, respectively, when compared to RCP2.6. Decreased dissipation rates and increased wave overtopping in forecasted climate conditions suggest the need for strategies to promote coral growth to facilitate high dissipation rates in the future. The results from our novel modelling approach have implications for the future habitability of exposed reef-lined coasts due to increased exposure to coastal flooding and island inundation.

Plain language summary

Coral reefs are essential for protecting coastlines from floods and waves, benefiting over 200 million people worldwide. We studied how waves change as they approach coral reefs, focusing on the forereef zone where wave transformation is most significant during high-energy conditions. The shape of the forereef, specifically the spur and groove (SaG) morphology, plays a crucial role in how much wave energy is dissipated and how much water spills over the reef.

Using a digital representation of waves over accurate reef shapes (known at bathymetry), we simulated wave dissipation rates comparable to real-world SaG studies. Our findings emphasize the importance of accurate representations of forereef shapes in models to predict wave energy dissipation, as they consider critical features such as SaG which affect how waves transform and lose energy.

Next, we investigated how wave energy dissipation and overtopping might change under different future climate scenarios. We considered low and high emission scenarios (RCP2.6 and RCP8.5) from the IPCC AR5 report and a total disaster scenario (TD) for the year 2100, factoring in changes to forereef elevation, wave power, and sea-level rise.

Under the low emission scenario (RCP2.6), with a slight increase in wave heights and water levels, we observed a doubling of wave energy dissipation rates. However, under the high emission scenario (RCP8.5) and the total disaster scenario (TD), dissipation rates decreased significantly compared to RCP2.6, resulting in more water moving over the reef crest during storms. This suggests that future climate conditions may lead to increased flooding and inundation on reef-lined coasts, putting communities at risk.

In summary, our study highlights the benefits of using accurate reef shapes in simulating wave energy dissipation on coral reefs. Accurate bathymetries can incorporate features such as spurs and grooves of different shapes, which modify wave dissipation. Wave energy dissipation changes when climate change projections are incorporated into the simulations leading to an increase in energy passing over the forereef.

1. Introduction

Coral reefs provide many ecosystem services including coastal hazard protection from ocean waves, with over 200 million people worldwide depending on the stability of this service (Ferrario et al., 2014). Coral reefs are topographically complex structures which contribute to the frictional dissipation of waves, however this has been studied in greater details on the reef crest and reef flat (Ferrario et al., 2014; Monismith et al., 2015; Péquignet et al., 2014; Yao et al., 2020) than on the high-energy environments of the forereef slope (Acevedo-Ramirez et al., 2021; Duce et al., 2014, 2016, 2022; Monismith et al., 2013; Sheppard, 1981). Yet, wave breaking on the forereef slope is the dominant form of wave energy dissipation under high-energy conditions (Osorio-Cano et al. 2018) suggesting that it is a critical region for coastal protection (Quataert et al. 2015a). High dissipation rates on the forereef are controlled by forereef morphology such as spurs and grooves (SaG) (Monismith et al., 2013; Osorio-Cano et al. 2018).

SaG are shore-normal elongate ridges (spur) and troughs (groove) on the forereef slopes of many coral reefs (Duce et al., 2016). Their size, spacing and orientation are typically aligned with incident waves and consequently the morphometric classification of SaG (Duce et al., 2016) reflects the influence of waves in their formation (Table 1). High energy forereefs feature more defined SaG than low-energy ones (Duce et al., 2016; Rogers et al., 2013). Recent research shows high-relief (up to 10 m) spurs in the Mexican Caribbean have a large influence over wave transformation, with dissipation in the SaG zone contributing a 35% in wave energy flux. Wave energy flux on the forereef occurs mostly in the sea-swell frequency band (> 0.04 Hz). While infragravity waves (0.004-0.04 Hz) are important to wave transformation over reef flats and in lagoons (Cheriton et al. 2016), field measurements of waves over SaG have shown negligible energy in the infragravity bands (Duce et al. 2022). A recent investigation into SaG morphology demonstrates that SaG are not optimised to maximise wave energy dissipation, with their morphology dissipating energy while allowing energy propagation (and water, nutrients, and oxygen) to facilitate coral growth in the lagoon (Johannsen et al., in review). Further field investigations are required but have been limited by the difficulty of accessing highly exposed and turbulent forereef slopes (Sheppard 1981; Sous et al. 2022).

SaG morphologies have been overlooked in both physical (e.g., Buckley et al., 2016) and numerical models (e.g. Baldock et al., 2020; Monismith et al., 2013; Osorio-Cano et al., 2018) of forereef wave attenuation. For instance, numerical models that include SaG morphologies typically use idealised bathymetries (e.g. da Silva et al., 2020; Rogers et al., 2013) with simplified morphologies that overlook the irregularity and diversity of SaG. Consequently, the impact of SaG morphologies (Table 1) on wave attenuation is poorly understood (Duce et al., 2022; Monismith et al., 2013; da Silva et al., 2020).

Table 1: Morphological categorisation of SaG (Duce et al., 2016).

Deep and Disconnected (DaD)	Grooves are disconnected from the reef crest and appear in deeper water (>5.5m) with limited hydrodynamic energy
Exposed to wave energy (EWE)	This morphology is heavily governed by the wave climate. Grooves are oriented perpendicular to incoming wave crests.
Log and protected (LaP)	Grooves are longer (>50m) and wider than more exposed grooves
Short and protected (SaP)	These grooves are narrower and shorter than Class 3.

Studies have shown that forereef morphologies including SaG will be impacted by climate change (Castillo et al., 2012; De'Ath et al., 2012; Hughes et al., 2018) likely resulting in reduced coastal protection (Baldock et al., 2014; Ferrario et al., 2014; Quataert et al., 2015; Sheppard et al., 2005) and increased wave overtopping (Amores et al. 2022; Beetham and Kench 2018). Most notably, a loss of structural complexity (roughness) in forereefs will reduce bed friction impacting wave attenuation (Baldock et al., 2014; Harris et al., 2018; Monismith et al., 2015; Rogers et al., 2016). These impacts are exacerbated by relative sea-level rise, changes in regional wave power (Meucci et al., 2020; Reguero et al., 2019) and modification and intensification of storm climates (Knutson et al., 2015) which all modify wave transformation processes on forereefs.

The overall aim of this paper is to provide understanding of present day and forecasted wave attenuation by SaG on coral reefs. Both of which are critical for coral reef management plans and climate change adaptation strategies. To achieve this, we first identify the benefits of high-resolution LiDAR-derived bathymetries in numerical wave models. Then we employ these models to determine how SaG of different morphological class affect the dissipation of wave energy. Finally, we investigate the effects of climate change on wave energy dissipation over SaG.

2. Methods

2.1 Study Site

One Tree Reef (OTR) (23°30'S, 152°06'E) is located 84 km offshore of the NE Australian mainland in the Capricorn Bunker Group, in the southern Great Barrier Reef (GBR) (Figure 1a). OTR is a lagoonal platform reef with semi-diurnal tides with a mean spring tidal range of 3 m. The entire forereef of OTR features SaG (Duce et al., 2016). The mean significant offshore wave height, $H_{s,mean}$ of 1.7 m (Smith et al., 2022) is typically generated from persistent SE trade winds that dominate the Coral Sea for over 70% of the year (Jell and Webb, 2012). Consequently, the south-eastern forereef is the most exposed to ocean swells (Figure 1b). We considered two study sites featuring SaGs of varying morphological class (Table 1) on the eastern and southern side of OTR (henceforth labelled OE and OS respectively) (Figure 1b, Table 1).

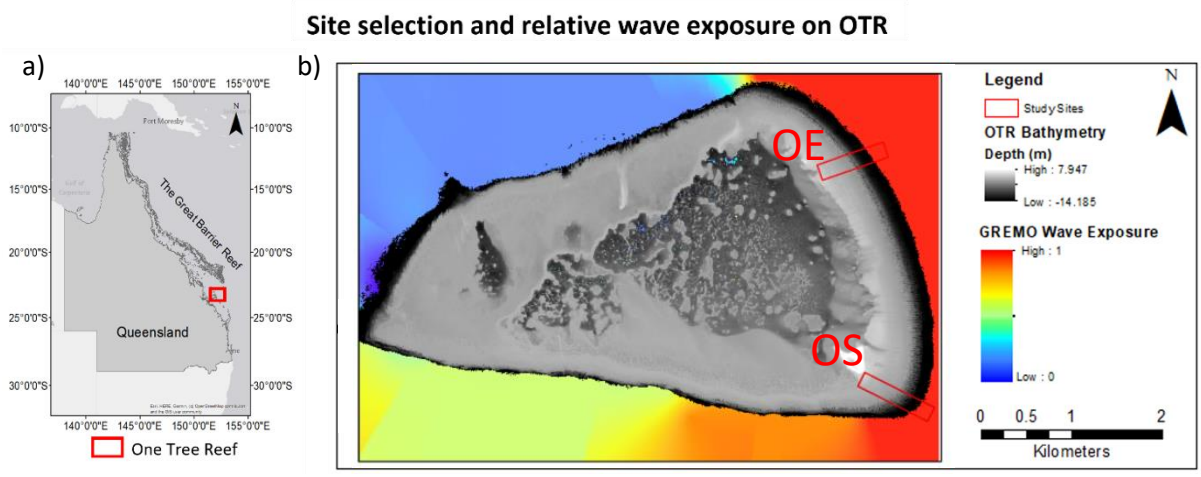

Figure 1: a) One Tree Reef (OTR) in the Southern Great Barrier Reef, and b) Study site locations for OTR East (OE) and OTR South (OS) and relative wave exposure (Pepper and Puotinen 2009).

2.2 SaG morphometric analysis

We determined morphometric parameters for SAG in the two study sites including length, depth, width, and others (Table 2) from analysis of LiDAR derived bathymetry and used them to classify the SAG following the categorical framework of Duce et al. (2016) (Table 1).

137 Table 2: Morphometric parameters of SaG adapted from Duce et al. (2016).

Morphometric parameter	**Method**
Length (L)	Path distance along the groove (m)
Depth (D)	The vertical distance between the lowest point in the groove and the highest point on the neighbouring spur is calculated at four depths below sea level (-2, -4, -6, and -8 meters).
Width (W)	Groove width is measured as the horizontal distance between its walls at half the depth, along isobaths of -2, -4, -6 and -8 m.
Orientation (θ)	Azimuth of straight line between maximum onshore and offshore extents of groove
Sinuosity (S)	Ratio of straight-line distance (D) to path length (L) such that: $S = D/L$
Wavelength (γ_{sag})	The horizontal distance between the highest points of adjacent ridges, parallel to isobaths, measured at depths of -2, -4, -6, and -8 meters below mean sea level.

138

139 2.3. Wave transformation modelling (XBeach)

140 We used XBeach (Roelvink et al., 2015) in Surf Beat mode to understand hydrodynamics and wave
141 attenuation over SaG because it has been extensively validated on complex coral reef bathymetries
142 (Harris et al., 2018; Lashley et al., 2018; Quataert et al., 2015, 2020; da Silva et al., 2020).

143 2.3.1 Bathymetric Grids

144 We merged data from a 0.5 m resolution Airborne LiDAR survey (Harris et al., 2023) to a depth of 14
145 m, and a 30 m resolution bathymetry survey (Beaman, 2017) to a maximum depth of 20 m (Figure
146 2). This maximum depth was selected to capture all depth-limited wave breaking within the model
147 and was based on historical wave heights for OTR considering,

Eq. 1

148 $$H_{max} = \gamma \cdot (h + \delta H_{rms})$$

149 where, γ is the breaker index, δH_{rms} is some fraction δ of the root mean square of the wave height.

150 The breaker index was held constant across the reef at $\gamma = 0.55$, reflecting the conservative

151 estimation ($\gamma = 0.55$) of (Duce et al., 2022) and within the ranges determined by Harris et al. (2018).

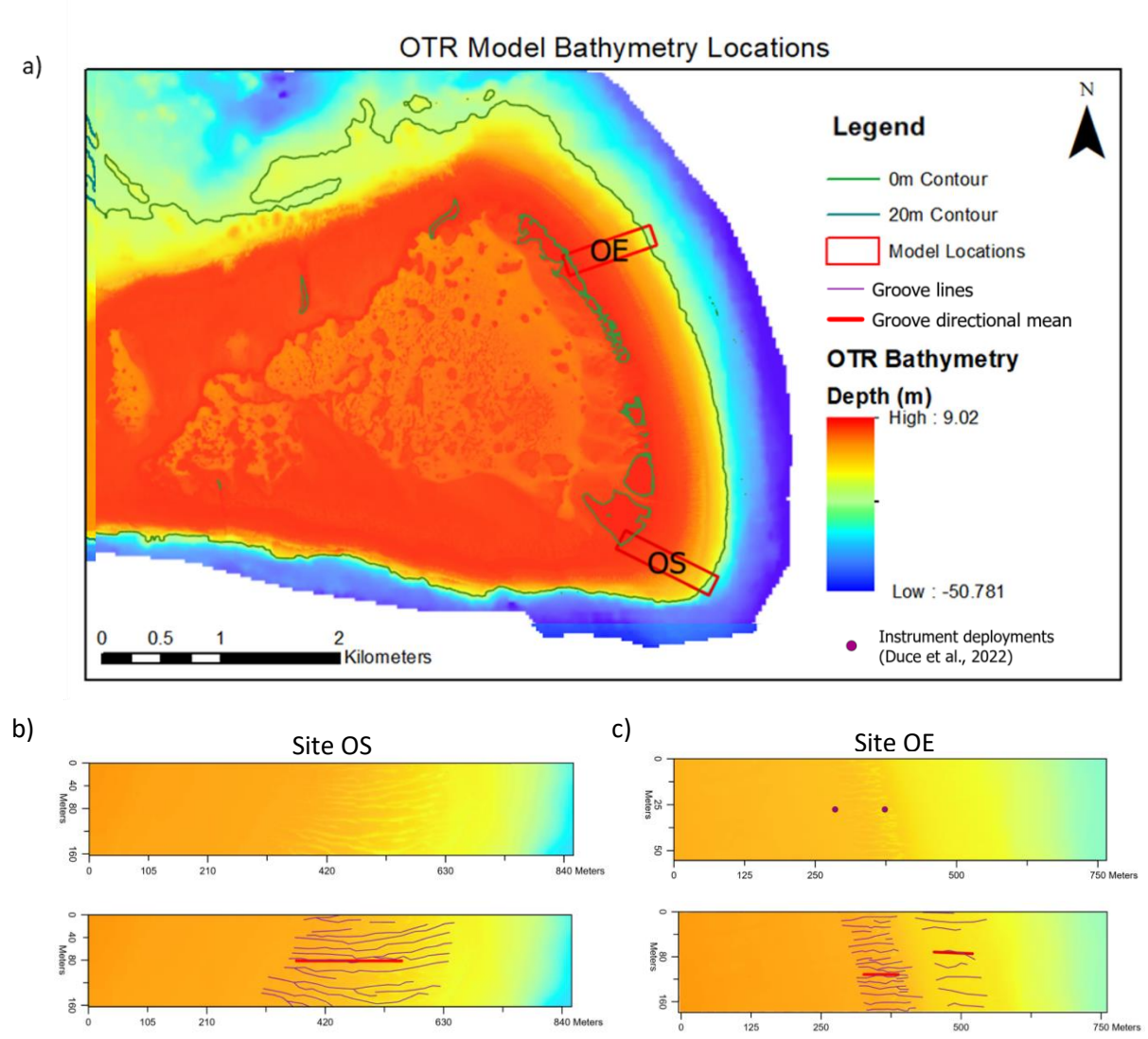

152

153 *Figure 2: a) The bathymetric grids used in wave models from two study sites on the eastern (OE) and*

154 *southern (OS) exposed forereefs of on One Tree Island. Grooves are shown in purple with the*

155 *directional mean of SaG shown in red.*

156 The outer boundaries of the bathymetric grids were oriented to align mean groove headings with

157 incident waves (Figure 2b and c), following field observations (Duce et al., 2014; Munk and Sargent,

1948; Shinn, 1963) and other wave transformation models constructed over SaG (Rogers et al., 2013; da Silva et al., 2020) (Figure 2b). Offshore boundaries were set beyond the maximum breaker depth for modelled wave heights (20 m: Eq. 1) and the onshore boundaries at present-day 0 m MSL contour (Figure 2b, c). Consequently, grids for each site are of different length and width (Figure 2b).

2.3.2 Climate change projections

We considered four climate change scenarios projected for the year 2100 including critical climate impacts to wave energy dissipation on coral reefs: sea-level change, reef health and wave energy conditions. The climate change scenarios are based on IPCC AR5 and include (1) the *present-day* scenario considering no change to current environmental factors, (2) the *low* (RCP 2.6) and (3) *high* (RCP8.5) emission scenarios from the AR5 IPCC report (Shukla et al., 2019), and (4) a *total disaster* (TD) scenario included to represent a high carbon future.

2.3.2.1 Changes to Sea Level

We used IPCC AR5 sea-level rise (SLR) rate of 3 mm/yr (Shukla et al., 2019). Under the *low* and *high* emission scenarios (RCP2.6 and RCP8.5) SLR is expected to reach up to 10-20 mm/yr. Subsequently, we have included SLR of 0.43 m (RCP2.6) and 0.84 m (RCP8.5) for the year 2100 (Shukla et al., 2019). Human stressors (e.g., infrastructure development and human-induced habitat degradation) are also likely to contribute to increases in local SLR (Shukla et al., 2019). An additional 1 m of eustatic SLR was included for our *total disaster* (TD) scenario to reflect significant changes to climate conditions and non-climatic anthropogenic stressors (Shukla et al., 2019) (Table 3). The total sea-level increase in each of the models (Table 3) was determined by the sum of eustatic and local sea-level changes, and the vertical accretion and erosion of the reefs.

2.3.2.2 Reef Morphological Changes

Reef morphological changes have been simplified into three key characteristics, reef vertical accretion, erosion, and structural complexity. A forecasted vertical accretion rate of 2 mm/yr was used based on field measurements from coral reef cores from across the GBR (Dechnik et al., 2015; Sanborn et al., 2020), Western Australia (Perry et al., 2018), Tahiti (Buddemeier and Smith, 1988),

the Maldives (Kench et al., 2022), Indo-Pacific averages compiled by Montaggioni (2005) and the Solomon Islands (Saunders et al., 2016). Alternatively, erosion of forereefs can occur due to the physical removal of coral and framework by storms and high wave energy (Madin and Connolly, 2006). This is most evident on degraded coral reefs where erosion has been observed at 6 mm/yr (Eakin, 1996; Sheppard et al., 2005). We used a conservative estimate of 2.6 mm/yr (0.2 m by 2100) of reef erosion for RCP 8.5 and a maximum of 6.4 mm/yr (0.5 m by 2100) of erosion under a TD scenario, modelled as a uniform decrease in elevation over the simulated domain. The resulting sea level was determined by combining projected rates of SLR with erosion and accretion values for each scenario (Table 3).

To simulate a loss in forereef structural complexity, we altered the dimensionless wave friction factor (f_w) to replicate changes to coral structural complexity. In our study, f_w were linearly interpolated between $f_w = 0.9$ (healthy reef) to $f_w = 0.1$ (degraded or smoothed reef). For the *total disaster* (TD) scenario, which represents a degraded reef and a shift to a carbonate sand substrate we used $f_w = 0.01$ (Smyth and Hay, 2002) (Table 3).

2.3.3 Wave Input Parameters

Mean offshore wave conditions were determined by satellite altimeter observations over 30 years (1985–2015) using RADWave (Smith et al., 2020) (Table 3). A small region (0.6° x 0.4°) representing dense altimeter data tracks was identified on the eastern, exposed side of OTR (Figure S1). We determined site-specific model input wave heights (H_{model}) by combining offshore wave conditions with a relative wave exposure model, GREMO (GIS-based generic model for estimating relative wave exposure; see Figure 1b) following Pepper and Puotinen (2009),

$$H_{model} = K_r \; H_{offshore} \quad (1)$$

where, $H_{offshore}$ is the offshore wave height obtained from RADWave (Figure 1b and Figure S1) and K_r is the relative exposure coefficient, normalised between 1 (most exposed) and 0 (least exposed).

Finally, altimeter wave heights were compared to measured waves at the northern forereef at OTR (Duce et al., 2022).

2.3.4 Changes to wave climate

We increased offshore model wave heights ($H_{offshore}$) for future climate change scenarios (Table 3) with wave periods (T_{model}) determined for a fully developed sea-state from the Joint North Sea Wave Project (JONSWAP) spectrum (Young, 1992). Storm waves were calculated from the maximum wave height observed in RADWave altimeter data. The final model wave heights were dependent on forereef location and relative exposure to wave energy determined by Eq. 1.

Table 3: Model input parameters are presented for three study sites, two wave conditions and four forecasted climate outcomes for the year 2100. A total of 16 unique models were run.

Site	Climate scenario	Wave Condition	$H_{offshore}$ (m)	Exposure Factor	H model (m)	T_{model} (s)	Friction factor	SLR (m)	Vertical Accretion (m)	Reef erosion (m)	Total change in MSL (m)
OS	Present day	Mean	1.34	0.985	1.3	5.74	0.9	0	0	0	0
	RCP 2.6		2.14				0.54	0.43	0.16	0	0.3
	RCP 8.5		2.14		2.1	7.26	0.1	0.84	0.1	0.2	0.99
	TD		2.14				0.01	1.84	0	0.5	2.34
	Present day	Storm	4.8		4.7	10.87	0.9	0	0	0	0
	RCP 2.6						0.54	0.43	0.16	0	0.3
	RCP 8.5		5.6		5.5	11.74	0.1	0.84	0.1	0.2	0.99
	TD						0.01	1.84	0	0.5	2.34
OE	Present day	Mean	1.34	0.9042	1.2	5.5	0.9	0	0	0	0
	RCP 2.6		2.14				0.54	0.43	0.16	0	0.3
	RCP 8.5		2.14		1.9	6.96	0.1	0.85	0.1	0.2	0.99
	TD		2.14				0.01	1.84	0	0.5	2.34
	Present day	Storm	4.8		4.3	10.42	0.9	0	0	0	0
	RCP 2.6		5.6				0.54	0.43	0.16	0	0.3
	RCP 8.5		5.6		5.1	11.25	0.1	0.84	0.1	0.2	0.99
	TD		5.6				0.01	1.84	0	0.5	2.34

2.3.5 XBeach model outputs

Each model was run for a total of 300 seconds, and we analysed the outputs of Xbeach for water surface elevation (zs), total dissipation rate (D), and dissipation rate due to bed friction (D_f) to obtain wave energy dissipation rates and wave overtopping. Total dissipation was used to compare Xbeach results with field measurements and to determine dissipation by breaking (D_b) such that $D_b = D - D_f$. As models are two-dimensional (x, y spatial domains) and evolve through time (t), we calculated mean and peak dissipation rates across t and x domains for the entire bathymetric grid. Mean dissipation rates were also taken between two points where hydrodynamic data sampled by Duce et al. (2022). Wave overtopping was calculated as the difference between the initial water level at the reef crest and the maximum water level at the reef crest during each model run.

3. Results

3.1 SaG morphometric analysis

SaG morphometrics were quantified for 123 grooves across the two study sites (Table 3). Grooves at the southern site (OS) were on average 3 times longer, 1.4 times deeper and 1.3 times wider than those at the eastern site (OE) (Table 3). Using the morphometric classification of Duce et al. (2016), the exposed to wave energy (EWE) grooves were the most common across three of the four sites (100 of 123 SaG) (Table 3). Deep and disconnected (DaD) grooves were present on the lower forereef platform of site OE.

Table 4: Morphometric parameters and classes of SaG at two study sites.

	Mean SaG Morphometric Parameters					Quantity of SaG Classes by Site			
Site	**Length (m)**	**Sinuosity**	**Orientation (Deg)**	**Depth (m)**	**Width (m)**	**DaD**	**EWE**	**LaP**	**SaP**

OS (south)	187.12	0.99	116.73	1.95	4.02	0	40	0	0
OE (east)	63.18	0.99	71.5	1.38	3.12	23	60	0	0

3.2 Wave transformation over LiDAR derived bathymetry

The peak dissipation rates under present day conditions, taken as the maximum dissipation across all axes (x, y, t), were 463.9 and 946.3 W/m^2 at sites OE and OS respectively (Figure 4). Wave energy dissipation due to bed friction was dominant in present day scenarios over dissipation due to wave breaking (Figure 4b and d). Between the two locations of field measurements conducted by Duce et al., (2022) (Figure 2c) the mean dissipation rate was 10.6 W/m^2, the maximum dissipation rate of 463.9 W/m^2 occurred during this zone. Wave energy dissipation by bed friction contributed 78% of energy at the site OE before waves reached the reef crest, 67% at site OS in the upper forereef slope. The maximum wave energy dissipation due to wave breaking constituted 22%, and 32% of total dissipation at site OE and OS respectively (Figure 4b, d).

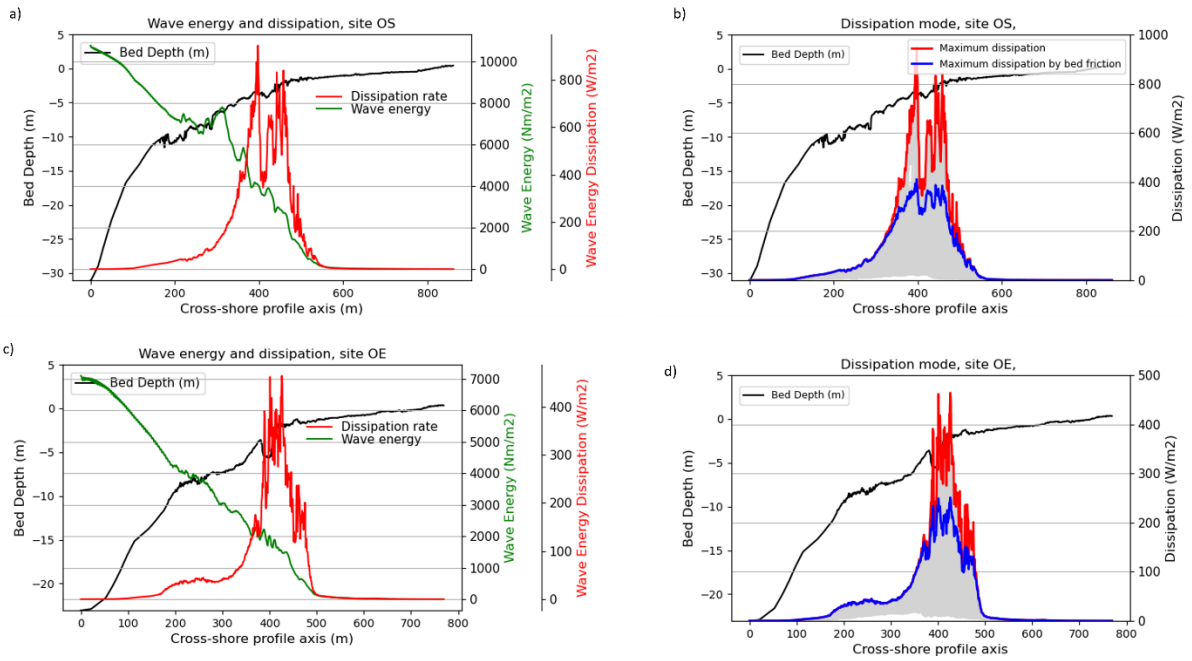

Figure 4: Wave energy (green) and maximum wave energy dissipation at site OS (a) and site OE (c). Maximum dissipation and maximum dissipation by bed friction (blue) for site OS (b) and site OE (d). Note different scale bars are used for each site.

3.3 Wave transformation under future climate change projections

Wave transformation was found to vary greatly among models depending on climate change scenario, SaG morphometrics, and wave exposure. The largest influence on wave energy dissipation across the two sites was the reduction of the bed friction factor (f_w), increased water depth, and increased wave height. Total wave energy dissipation and dissipation due to bed friction changed at both sites for all future climate scenarios (Table 3).

Mean and peak dissipation rates were computed for each site across all three climate scenarios (Table 3, Figure 5). When comparing dissipation rates from present day to RCP2.6 for the year 2100, mean dissipation increased by 187% at site OS (4.4 to 12.5 W/m^2) and maximum dissipation increased by 59.7% (946.3 to 1511.4 W/m^2) (Figure 5a and b). At site OE, mean dissipation rate increased by 208.6% (2.5 to 7.8 W/m^2) and maximum dissipation increased by 217.7% (463.9 to 1473.4 W/m^2) (Figure 5d and e).

When comparing RCP2.6 to RCP8.5 we found a decrease in mean dissipation across site OS of 18.1% (12.5 to 10.6 W/m^2) and an increased in the max dissipation rate of 23.2% (1511.4 to 1966.9 W/m^2). Site OE retained at high mean dissipation rate from RCP2.6 to RCP8.5, increasing a further 11.7% (7.78 to 8.81 W/m^2) and an increase of 19.3% to peak dissipation rate (1473.42 to 1824.70 W/m^2).

When comparing to RCP8.5, the TD scenario, mean dissipation rates decreased by 66.2% (10.61 to 3.58 W/m^2) at site OS and a decrease in peak dissipation of 31.8% (1966.89 to 1340.93 W/m^2) (Figure 4b and c). At site OE, mean dissipation decreased by 86.2% (8.81 to 1.21 W/m^2) and peak dissipation rate decreased by 75.4% (1824.7 to 448.24 W/m^2) (Figure 5e and f).

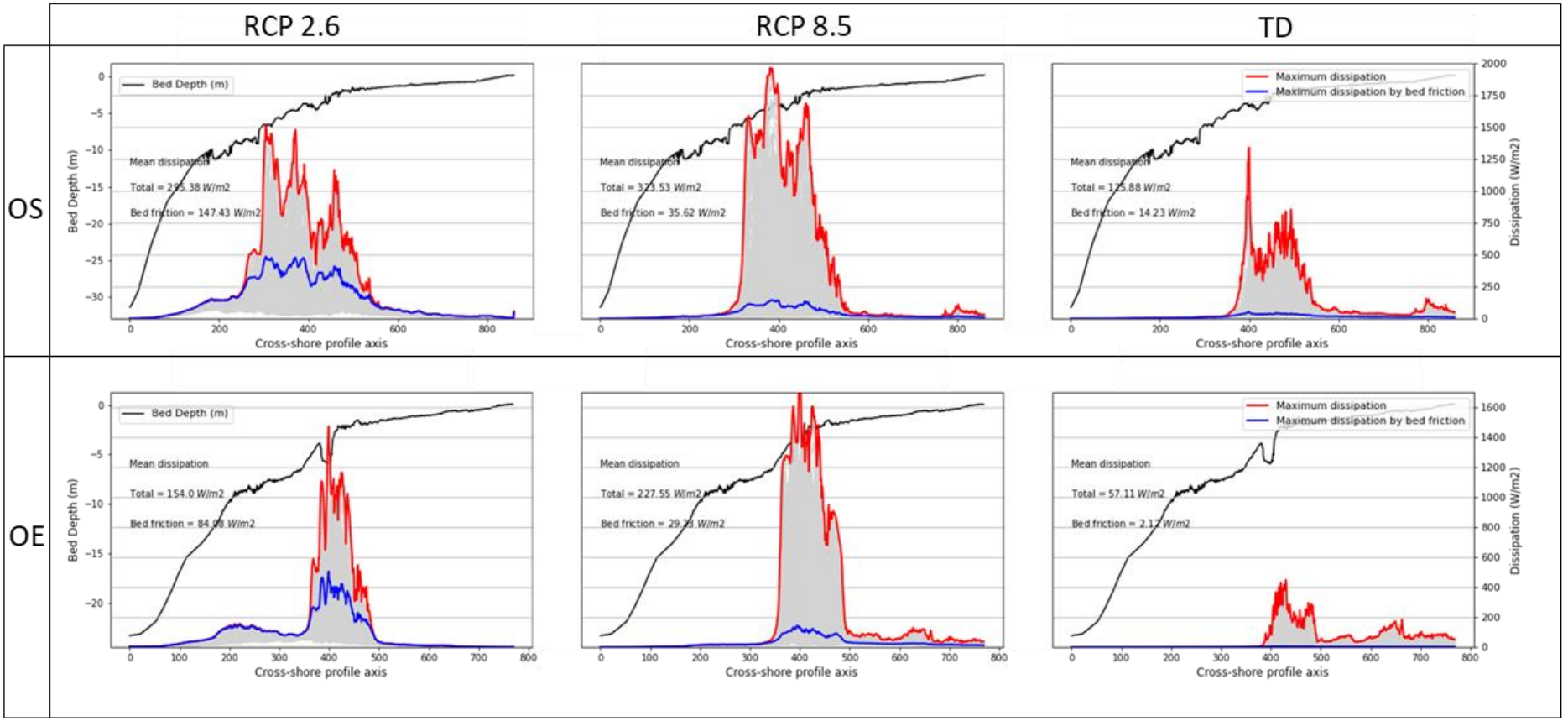

273

274 *Figure 5: Maximum wave energy dissipation (blue) and dissipation due to bed friction (red) for across the x and time domains, for Site OS under a) RCP 2.6, b)*
275 *RCP 8.5 and c) TD climate change outcomes. for site OE under d) RCP 2.6, e) RCP 8.5 and f) TD climate change outcomes. Mean wave energy dissipations are*
276 *provided numerically for each plot. Note Y axis are unique for each study site to highlight relative differences in dissipation under variable climate change*
277 *outcomes.*

Under present-day conditions, bed friction is dominant, contributing 98% and 99% of total wave energy dissipation (Figures 5 and 6). Comparing RCP 2.6 to RCP 8.5, the OS site decreased frictional dissipation by 57% and at site OE this was 42% (Figure 5 and Figure 6). In this case, dissipation by wave breaking increased by an average of 659% for both sites. This results in a shift in the dominant form of wave energy dissipation (Figure 6). Comparing RCP2.6 to the TD scenario, mean frictional dissipation (D_f) decreases by 82.5% at site OS and 95.8% at site OE while wave breaking remains marginally greater by 0.1% (OS) and 1.5% (OE) in the TD scenario. Despite this, mean total wave energy dissipation (the sum of frictional and wave breaking dissipation rates) decreases by 71.4% (OS) and 84.4% (OE).

a)

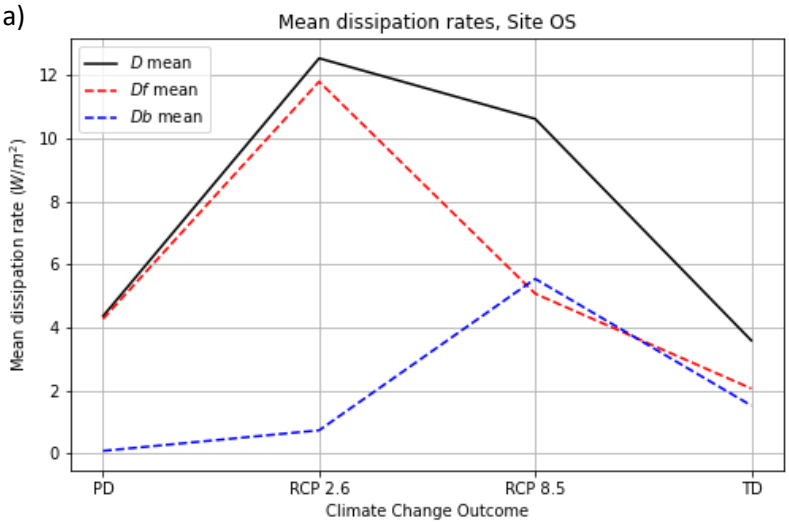

b)

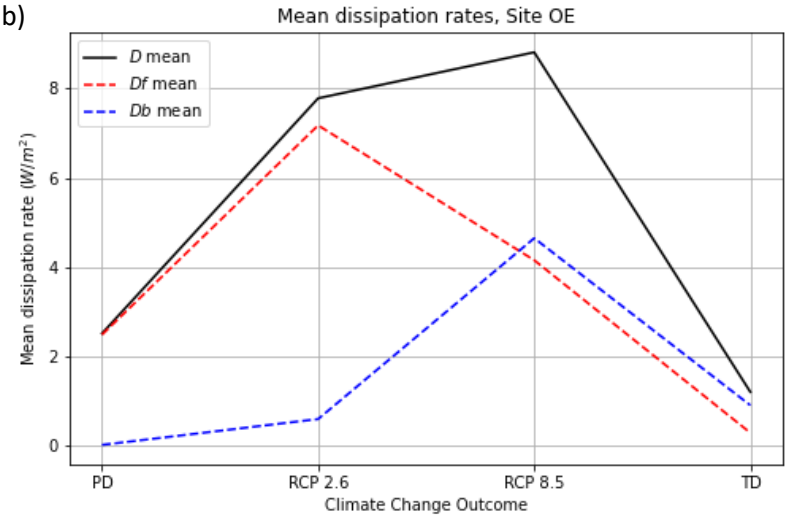

Figure 6: Mean total dissipation (D mean) for OS (a) and OE (b) study sites and mean dissipation by bed friction (Df mean) and wave breaking (Db mean) for each climate change scenario (see Table 3).

We calculated wave overtopping for both sites under present day conditions and three climate change scenarios considering both mean and storm wave conditions (Table 2). For mean wave conditions, wave overtopping in the present-day model was near zero (0 and 0.1 m at site OS and OE, respectively). Wave overtopping increase for all forecast climate change scenarios (Figure 6). We calculated overtopping of 0.4 m at site OS and 0.1 m at site OE for RCP 2.6 with larger increases to 0.4 m (OS) and 0.7 m (OE) for RCP8.5. The high emissions scenario (TD) had the highest overtopping of 2.1 m (OS) and 2.0 m (OE).

Storm wave conditions increased overtopping compared to mean wave heights in all cases (Figure 7; Table 2). Under present-day conditions, wave overtopping was greater than for mean wave conditions at 1.25 and 0.5 m for site OS and site OE respectively. Under forecast climate change scenarios, storm waves did not significantly impact overtopping under RCP2.6 compared to present day conditions despite an increase in wave height of 3.5 m. Overtopping under RCP8.5 was 2.1 m at site OS and 1.4 m at site OE which increased significantly to 3.5 m and 3.9 m in pessimistic TD models at each site respectively.

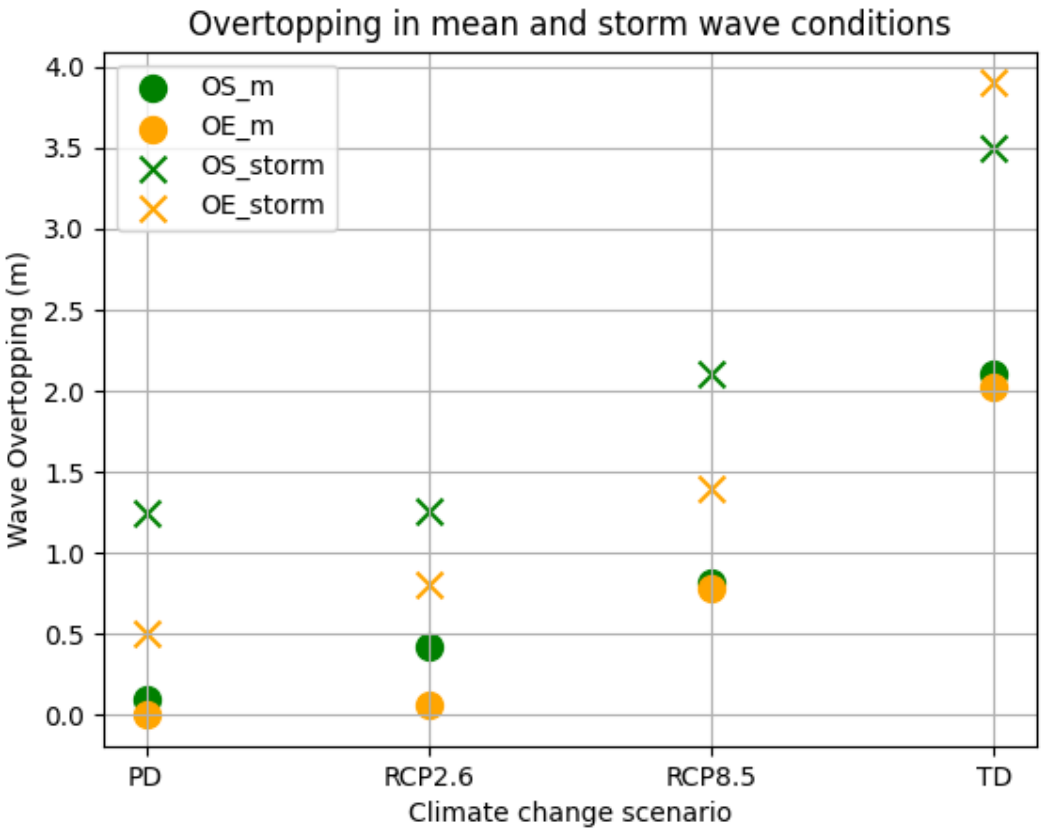

Figure 7: Wave overtopping at both sites under mean (OS_m and OE_m) and storm (OS_storm and OE_storm).

4. Discussion

4.1 Benefits of high-resolution LiDAR-derived bathymetries in numerical wave models

Our models of wave transformation over LiDAR-derived bathymetries focus on the influence of SaG morphology on wave energy dissipation and overtopping. Under mean wave conditions we calculated average dissipation rates across the entire forereef profile of 3.61 W/m^2 at site OS and 2.52 W/m^2 at site OE for offshore wave heights of 1.3 m and 1.2 m respectively. This calculation is made across the entire reef profile representing 862 m and 770 m respectively (Figure 2b, c). Field measurements of wave energy dissipation conducted at OTR were taken at the same site as OE presented in this study (Figure 2c) (Duce et al. 2022). We determined a mean dissipation rate of 10.6 W/m^2 across 60 m between the two instruments, almost entirely due to bed friction (Figure 4 d).

Duce et al. (2022) recorded mean dissipation rates of 20 W/m^2 with wave heights of H_s = 0.78 m and T_p = 5 seconds. Differences in the recoded and modelled data at this site may be attributed to the incident wave direction (N-NE during the deployment period) which was not completely aligned with SaG as modelled here. These results compare with data obtained on a fringing reef in Ipan (Guam) which also featured SaG on the forereef (Péquignet et al., 2011). Between two sensors placed 55 m apart inside a 5 m deep groove, the dissipation rate was 25 W/m^2 for offshore wave heights of 1-2 m (Péquignet et al., 2011). Monismith et al. (2015) identified comparable dissipation rates of 25 W/m^2 on a forereef in Palmyra (Kiribati) between instruments 50 m apart for incident wave heights of 1 m. Monismith et al. (2013) determined rates of 22 W/m^2 across a forereef at Mo'orea (French Polynesia) with instruments located 50 m apart and wave heights of 0.3 to 0.5 m. Dissipation rates for each of these studies are assumed to be due to bed friction with constant dissipation between the instruments. Our results indicate that the dissipation rate across the forereef is heterogenous and controlled by the bed morphology (e.g. Figure 5 a). The use of real bathymetries in modelling efforts can elucidate the heterogeneity of dissipation rates on forereefs.

Using a real bathymetry, our study demonstrates the influence of groove sinuosity on wave energy dissipation by breaking. Our results show that shore-normal waves interact with spur walls that do not perfectly align with incoming swells. Indeed in our study, the mean groove heading was used to align the bathymetric grids to the oncoming waves (Figure 2b), consistent with field observations (Duce et al., 2020; Munk and Sargent, 1948). Despite this, variation in headings between grooves and the sinuosity of individual grooves produces steep irregularities in the forereef slope that have a large impact on the oncoming waves, playing a significant role on both dissipation by wave breaking and bed friction. The straight and shore normal SaG identified in this analysis (mean sinuosity of S=0.99, where 1 is a perfectly straight groove) (Table 4) are representative of groove sinuosity across the southern Great Barrier Reef. For example, observations of 12,102 grooves in the GBR and South Pacific show a mean groove sinuosity of S = 0.98 (Duce, 2017). Despite remarkable regional consistency in groove morphology, we observed that even small deviations from perfect shore-

normal grooves are significant to wave transformation on the forereef. A more sensitive measure for groove sinuosity may allow for a better understanding of forereef hydrodynamics. Further investigation into SaG sinuosity effects should consider the natural sinuosity of SaG derived from high resolution digital elevation models to account for these effects.

4.2 Effects of SaG from different morphological classes on wave energy dissipation

The most wave exposed site (southern site, OS) has the highest average dissipation rates of 71.5% over 300 m SaG zone due to bed friction (Figure 4a). The long (mean length of 187.12 m) and deep (mean depth of 1.95 m) exposed to wave energy (EWE) grooves at this exposed site may explain how this high average dissipation rate occurred (Table 1). The length of EWE SaG creates surfaces of high frictional drag that extend the zone of frictional dissipation and contribute to high average dissipation rates (Figures 4a and 5). Shore normal currents occurring in the long and deep grooves have also been observed and facilitate high rates of dissipation (Rogers et al., 2013). We demonstrate under present-day conditions that bed frictional dissipation is dominant in dissipating wave energy before breaking occurs at the reef crest (Figure 4a and c). Bed frictional dissipation represents 98.0% and 98.9% of total dissipation at site OS and OE respectively (Figure 4a and c). This is consistent with field research conducted at OTR (Duce et al., 2022) and in other high-energy settings (Lowe et al., 2005; Monismith et al., 2015; Rogers et al., 2017). For example, under mean wave conditions at Palmyra (Kiribati), a high bed friction coefficient (f_w =1.8) facilitated greater wave energy dissipation due to bed friction than from wave breaking (Monismith et al., 2015), which is consistent with field observations in Kaneohe Bay, Oahu, Hawaii (Lowe et al., 2005). Our results suggest that the modes of wave energy dissipation (frictional or breaking) are not only influenced by the wave conditions but also by the heterogenous morphology of the forereef slopes.

SaG morphology and consequently the morphological classes of Duce et al., (2016) can provide further explanations to the mode of wave energy dissipation (Table 1). Where grooves are shorter, they play a critical role in creating steep bathymetric gradients that induce wave breaking (Figures 4 and 8). This differs from previous SaG research (Acevedo-Ramirez et al., 2021) that showed wave

369 breaking being induced by the reef crest. Semi-exposed SaGs (represented here by site OE) are
370 typically shorter (mean length of 71.5 m) and shallower (mean depth of 1.38 m) than the most
371 exposed sites (site OS) and can include both exposed to wave energy (EWE) and deep and
372 disconnected (DaD) classes (Table 1). The seaward extent of the EWE grooves at semi-exposed
373 forereef sites (OE; Figure 4d) feature a steep bathymetric incline that produces the maximum wave
374 energy dissipation by wave breaking rate observed across all present-day models (1824.7 W/m^2,
375 Figure 5). As such, long spurs can facilitate frictional dissipation and short grooves can induce wave
376 breaking by introducing steep bathymetric inclines within the breaker zone of incident waves.

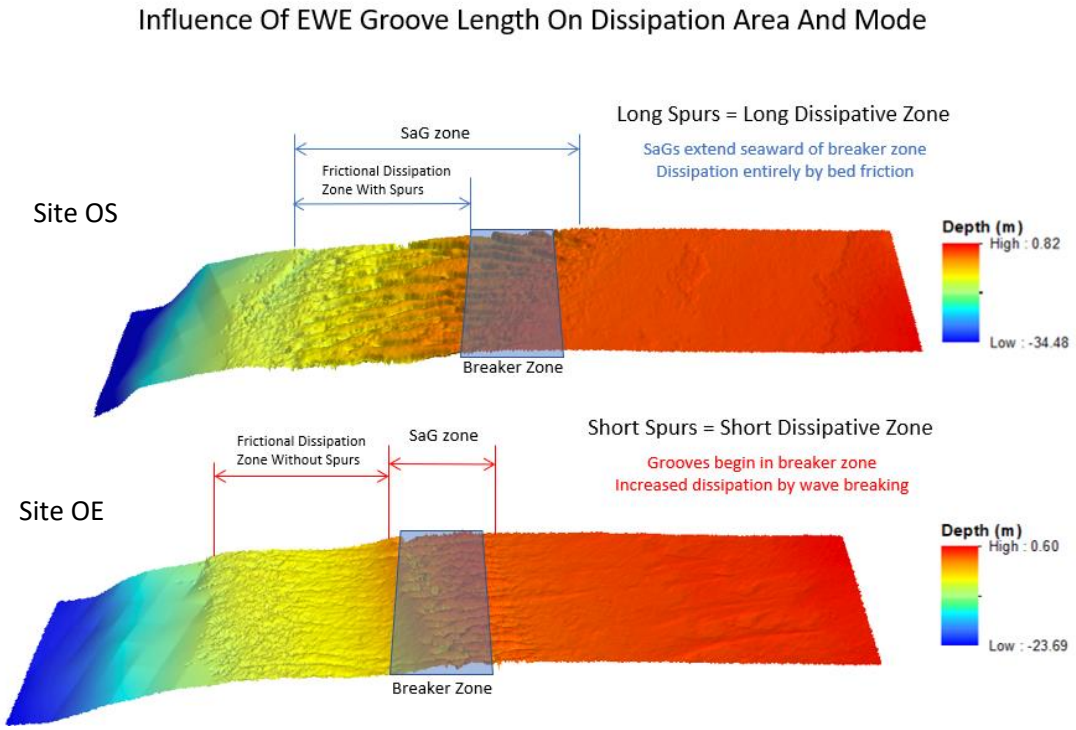

377

378 *Figure 8: A comparison between exposed and semi-exposed bathymetric profiles (site OS and site OE)*
379 *demonstrate the influence of the length of the SaG zone.*

380 The peak in wave energy dissipation at the shoreward of exposed to wave energy (EWE) grooves
381 highlights the complex interaction between forereef morphological evolution and wave energy
382 (Figure 4e). The seaward extent of EWE grooves is at a depth of 3.5 m, coincident with the mean
383 model wave height breaker depth for waves of 1.3 – 4.3 m (Figure 4, Table 2). As wave breaking

imposes forces on the structure of the reef (Massel & Gourlay, 2000; Storlazzi et al., 2005) the results presented here suggest that incident waves could be capable of modifying the EWE grooves in this zone, which is consistent with C14 and U-Th ages of SaG formations on the eastern forereef of OTR (Duce et al., 2020), suggesting an erosive origin for this grooves. Imposed climate change effects further elucidate the influence of grooves. Deep and disconnected (DaD) grooves at site OE exist below the typical wave base and have minimal interaction with present day wave energy. Supporting the previous findings that DaD grooves may be relict features, formed at an early stage during the Holocene transgression (Duce et al., 2016).

4.3 The impact of climate change on wave energy dissipation over SaG

Forecasted environmental changes decrease mean wave energy dissipation (Figure 5) which is consistent with other approaches (e.g., Quataert et al., 2015; Sheppard et al., 2005). In the simulations presented here, dissipation remains high between RCP 2.6 and RCP 8.5 as reduced dissipation by bed friction is balanced by an increase in dissipation by wave breaking (Figures 5 and 6). The difference between dissipation by bed friction and dissipation by wave breaking is the greatest at both sites for RCP 8.5, where water depth is still sufficient for wave breaking, yet the degradation of the reef reduces frictional effects (see Figure 9). A reliance on wave breaking dissipation is consistent with observations from high energy reefs of low structural complexity (Harris et al., 2018). Finally, dissipation is lowest where SLR is greatest (TD scenario) due to wave passing over the reef without breaking (Figure 9). Although the role of SLR is thought to be secondary in contributing to these changes (Harris et al., 2018), our models suggest that the combined impact of SLR and loss of structural complexity will lead to lowest dissipation rates (Figures 5 and 9) and highest wave overtopping (Figures 6 and 9) under future climate change scenarios.

Sea-level rise (SLR) shifts the region of high energy dissipation toward the reef-crest (Figure 5b, c and e, f). Bathymetric features that are submerged into the surf zone by rising relative sea level are likely

409 to influence wave breaking and frictional dissipation (Figure 5). This is evident in the shoreward
410 shifting dissipation zones (Figure 5) and as previous literature states (Massel and Gourlay, 2000) is a
411 threat to corals in this zone as wave breaking results in greater hydrodynamic forces on corals.
412 Corals previously protected from wave energy are likely to be species of lower mechanical strength
413 (Storlazzi et al., 2005). Under worse case scenarios (RCP 8.5) by the year 2100 it is likely that corals
414 of the same species may be weaker due to lower carbonate saturation in the water column (Eakin,
415 1996) or high frequency bleaching events (Hughes et al., 2017). Coral breakage is likely to occur here
416 and the corals that support a steep bathymetric incline with a high frictional coefficient responsible
417 for this peak in wave energy dissipation may have lower structural resilience by 2100 (Eakin, 1996).

418 High-energy SaG formations have been attributed to wave induced erosion, albeit at vastly different
419 timescales to sedimentary swash-zone features such as rip channels (Duce et al., 2020). It is possible
420 that climate change-driven increase in erosive forces promote further SaG development on
421 forereefs, which contributes to the dissipation of wave energy.

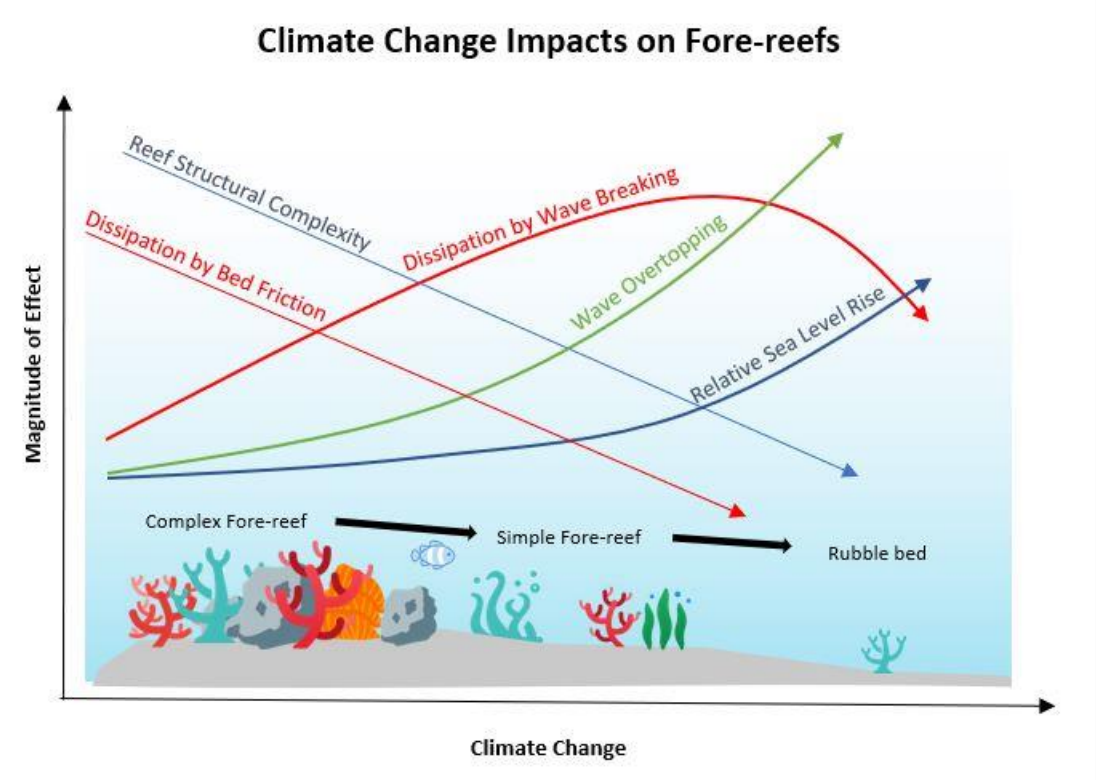

422

Figure 9: A conceptual diagram of changes to wave transformation on forereefs under increasing climate change impacts. Climate driven inputs including loss of reef structural complexity and relative sea-level rise are shown (blue). Dissipation rates (red) due to bed friction decreases, in response, dissipation due to wave breaking increases until water depth exceeds breaker depths. Wave overtopping (green) increases exponentially due to the combined effects of relative sea-level rise and loss of reef structural complexity.

4.3.2 Potential for wave overtopping with climate change

Wave overtopping exponentially increases with climate change due to the coupled effects of decreased bed friction and loss of dissipation due to breaking (Figure 7). Compared to mean wave conditions, the impact of storm waves results in increasingly greater overtopping when climate projections are increased. (Figure 7). This effect is persistent despite the increased wave energy dissipation at the semi-exposed forereef (site OE) under RCP 8.5 (Figure 4e). The primary control on wave overtopping is sea-level rise, which incorporates eustatic and local sources. Future work should include tidal effects, which would contribute an additional 1.5 m of water level at mean spring high tide at OTR (Harris et al., 2015). The magnitude of wave overtopping observed in the TD scenario at the exposed site (OS) of ~4 m is sufficient to entirely flood all backreef environments at OTR, including the low-lying coral island. This magnitude of wave overtopping would have significant impacts on coral reef islands and reef-lined shores(Fellowes et al. 2022; Storlazzi et al. 2015; Talavera et al. 2021). For example, 3.7 m of wave run up combined with sea surface elevation above a reef flat in Roi-Namur, Marshall Islands, was observed in flooding of inland area of the Island (Cheriton et al., 2016). Research elsewhere demonstrated that wave overtopping on reef islands in the year 2100 will be highly variable across due to variable reef vertical accretion and erosion rates (Beetham and Kench, 2018; Kench et al., 2022), but also due to the vertical accretion of coral reef islands (Kench et al., 2019, 2022; Masselink et al., 2020) which is controlled by sediment availability.

The combined influence of coral reef degradation and sea-level rise amplifies the occurrence of wave overtopping, thereby exposing communities located in the downwind direction of coral reefs to heightened risks of flooding (Harris et al., 2018; Quataert et al., 2015; Storlazzi et al., 2018). Notably, a maximum overtopping of approximately 4 m was measured here when the significant wave height reached 5.1 m. An examination of altimeter data reveals that within the 33-year data span, wave heights have not surpassed this threshold (95^{th} percentile wave height = 3.1 m) (Figure S1, supplementary material). Consequently, further investigation is required to determine the frequency of significant overtopping events at OTR.

5. Conclusion

This study combined numerical modelling and LiDAR-derived bathymetry to demonstrate the importance of forereef spur and groove (SaGs) morphologies in modifying wave energy. Results indicate that high resolution digital elevation models (< 1 m) can provide morphometric data to examine wave transformation on forereefs comparable to field studies. We show that groove sinuosity plays a role in wave transformation and should be considered in future research on wave dissipation on forereefs. This highlights the need for accurate bathymetries in future studies of forereef wave energy dissipation, as idealized bathymetries used in previous studies, using numerical or physical modelling, cannot provide results comparable to field studies.

We demonstrate that SaG morphological classes exhibit distinct dissipation characteristics, with some showcasing higher frictional dissipation and others exhibiting greater breaking dissipation. Notably, spur length emerges as a critical factor in enhancing dissipation by bed friction. Among the SaG morphological classes, exposed to wave energy (EWE) grooves have demonstrated the most substantial dissipation rates, while deep and disconnected (DaD) grooves contribute less to the dissipation process, particularly evident under future climate change scenarios.

Projected climate change conditions may lead to a decrease in wave energy dissipation on forereefs. Indeed, the climate change scenarios analysed demonstrated that changes in the mode of wave energy dissipation will likely occur. The most notable result was a decrease in dissipation by bed friction from 100% of dissipation under present day conditions to 48% under RCP 8.5. This is matched by a 52% increase in dissipation by wave breaking. Overall, we found a loss in wave energy dissipation under future climate change scenarios leading to increased wave overtopping, with the maximum overtopping occurring where dissipation was lowest. Forereef morphological adjustment to increased dissipation by wave breaking may expose corals to erosion, a process which has been linked to the formation of SaG. The results highlight the critical role of forereef morphology in wave energy dissipation and the need for measures to promote coral growth to facilitate future dissipation. The findings have implications for the modelling wave transformation over forereefs to provide insight into the future habitability of exposed reef-lined coasts.

6. Acknowledgements

We acknowledge the Gadigal people of the Eora Nation, the traditional owners of the land and waters where this research was conducted, and pay respects to their elders past, present and emerging. We acknowledge the cultural significance of the Southern Great Barrier Reef, where we conduct fieldwork, to the Tarebilang Bunda, Bailai, Gooreng Gooreng and Gurang Traditional Owners. Lachlan Perris was supported by an RTP scholarship from The University of Sydney and the research was partially funded by ARC Future Fellowship (FT100100215), ARC Discovery Program (DP220101125), and Geoscience Australia funding through the Marine Studies Institute at The University of Sydney.

Data Availability

XBeach version 1.22 (revision 4567) is used in this analysis and can be accessed through a Docker image available at https://hub.docker.com/r/tristansalles/docker2xbeach. Python codes used to interpret LiDAR derived bathymetry in XBeach can be found at https://github.com/Lachie-Perris/XBeach_coral. Satellite altimeter derived wave heights for the southern GBR are provided in csv format with python notebooks at https://github.com/Lachie-Perris/RADWAVE_OTI.

References

Acevedo-Ramirez, César A., W. Stephenson, S. Wakes, and I. Mariño-Tapia. 2021. "Wave Transformation on a Fringing Reef System With Spur and Groove Structures." *Journal of Geophysical Research: Oceans* 126(9):1–14. doi: 10.1029/2020JC016910.

Amores, Angel, Marta Marcos, Gonéri Le Cozannet, and Jochen Hinkel. 2022. "Coastal Flooding and Mean Sea-Level Rise Allowances in Atoll Island." *Scientific Reports* 12(1):1–12. doi: 10.1038/s41598-022-05329-1.

Baldock, T. E., A. Golshani, D. P. Callaghan, M. I. Saunders, and P. J. Mumby. 2014. "Impact of Sea-Level Rise and Coral Mortality on the Wave Dynamics and Wave Forces on Barrier Reefs." *Marine Pollution Bulletin* 83(1):155–64. doi: 10.1016/j.marpolbul.2014.03.058.

Baldock, T. E., Behnam Shabani, David P. Callaghan, Zhifang Hu, and Peter J. Mumby. 2020. "Two-Dimensional Modelling of Wave Dynamics and Wave Forces on Fringing Coral Reefs." *Coastal Engineering* 155. doi: 10.1016/j.coastaleng.2019.103594.

Beaman, R. J. 2017. "High-Resolution Depth Model for the Great Barrier Reef - 30 M."

Beetham, E., and P. S. Kench. 2018. "Predicting Wave Overtopping Thresholds on Coral Reef-Island Shorelines with Future Sea-Level Rise." *Nature Communications* 9(1). doi: 10.1038/s41467-018-06550-1.

Buckley, Mark L., Ryan J. Lowe, Jeff E. Hansen, and Ap R. Van Dongeren. 2016. "Wave Setup over a Fringing Reef with Large Bottom Roughness." *Journal of Physical Oceanography* 46(8):2317–33. doi: 10.1175/JPO-D-15-0148.1.

Buddemeier, R. W., and S. V. Smith. 1988. "Coral Reef Growth in an Era of Rapidly Rising Sea Level: Predictions and Suggestions for Long-Term Research." *Coral Reefs* 7(1):51–56. doi: 10.1007/BF00301982.

Castillo, Karl D., Justin B. Ries, Jack M. Weiss, and Fernando P. Lima. 2012. “Decline of Forereef Corals in Response to Recent Warming Linked to History of Thermal Exposure.” *Nature Climate Change* 2(10):756–60. doi: 10.1038/nclimate1577.

Cheriton, Olivia M., Curt D. Storlazzi, and Kurt J. Rosenberger. 2016. “Observations of Wave Transformation over a Fringing Coral Reef and the Importance of Low-Frequency Waves and Offshore Water Levels to Runup, Overwash, and Coastal Flooding.” *Journal of Geophysical Research: Oceans* 121(9):6762–78. doi: 10.1002/2016JC012132.Received.

De’Ath, Glenn, Katharina E. Fabricius, Hugh Sweatman, and Marji Puotinen. 2012. “The 27-Year Decline of Coral Cover on the Great Barrier Reef and Its Causes.” *Proceedings of the National Academy of Sciences of the United States of America* 109(44):17995–99. doi: 10.1073/pnas.1208909109.

Dechnik, Belinda, Jody M. Webster, Peter J. Davies, Juan-carlos Braga, and Paula J. Reimer. 2015. “Holocene ‘ Turn-on ’ and Evolution of the Southern Great Barrier Reef : Revisiting Reef Cores from the Capricorn Bunker Group.” *Marine Geology* 363:174–90. doi: 10.1016/j.margeo.2015.02.014.

Duce, Stephanie. 2017. “The Form, Function and Evolution of Coral Reef Spurs and Grooves.” University of Sydney.

Duce, Stephanie, Belinda Dechnik, Jody M. Webster, Quan Hua, James Sadler, Gregory E. Webb, Luke Nothdurft, Marcos Salas-Saavedra, and Ana Vila-Concejo. 2020. “Mechanisms of Spur and Groove Development and Implications for Reef Platform Evolution.” *Quaternary Science Reviews* 231. doi: 10.1016/j.quascirev.2019.106155.

Duce, Stephanie, A. Vila-Concejo, S. M. Hamylton, J. M. Webster, E. Bruce, and R. J. Beaman. 2016. “A Morphometric Assessment and Classification of Coral Reef Spur and Groove Morphology.” *Geomorphology* 265:68–83. doi: 10.1016/j.geomorph.2016.04.018.

Duce, Stephanie, A. Vila-Concejo, Sarah Hamylton, Eleanor Bruce, and Jody M. Webster. 2014. “Spur and Groove Distribution, Morphology and Relationship to Relative Wave Exposure, Southern Great Barrier Reef, Australia.” *Journal of Coastal Research* 70:115–20. doi: 10.2112/si70-020.1.

Duce, Stephanie, A. Vila-Concejo, R. J. Mccarroll, B. Yiu, L. A. Perris, and J. M. Webster. 2022. “Field Measurements from Contrasting Reefs Show Spurs and Grooves Can Dissipate More Wave Energy than the Reef Crest.” *Earth and Space Science Open Archive ESSOAr* 413(August 2021):108365. doi: 10.1016/j.geomorph.2022.108365.

Eakin, C. M. 1996. “Where Have All the Carbonates Gone? A Model Comparison of Calcium Carbonate Budgets before and after the 1982–1983 El Nino at Uva Island in the Eastern Pacific.” *Coral Reefs* 15(2):109–19. doi: 10.1007/bf01771900.

Fellowes, Thomas E., Ana Vila-Concejo, Shari L. Gallop, Mitchell D. Harley, and Andrew D. Short. 2022. “Wave Shadow Zones as a Primary Control of Storm Erosion and Recovery on Embayed Beaches.” *Geomorphology* 399:108072. doi: 10.1016/j.geomorph.2021.108072.

Ferrario, F., M. W. Beck, C. D. Storlazzi, F. Micheli, C. C. Shepard, and L. Airoldi. 2014. “The Effectiveness of Coral Reefs for Coastal Hazard Risk Reduction and Adaptation.” *Nature Communications* 5:3794. doi: 10.1038/ncomms4794.

Harris, Daniel L., Hannah E. Power, Michael A. Kinsela, Jody M. Webster, and Ana Vila-Concejo. 2018. “Variability of Depth-Limited Waves in Coral Reef Surf Zones.” *Estuarine, Coastal and Shelf Science* 211(December 2016):36–44. doi: 10.1016/j.ecss.2018.06.010.

Harris, Daniel L., Alessio Rovere, Elisa Casella, Hannah Power, Remy Canavesio, Antoine Collin, Andrew Pomeroy, Jody M. Webster, and Valeriano Parravicini. 2018. “Coral Reef Structural Complexity Provides Important Coastal Protection from Waves under Rising Sea Levels.” *Science Advances* 4(2). doi: 10.1126/sciadv.aao4350.

Harris, Daniel L., A. Vila-Concejo, J. M. Webster, and H. E. Power. 2015. “Spatial Variations in Wave

569 Transformation and Sediment Entrainment on a Coral Reef Sand Apron." *Marine Geology*
570 363:220–29. doi: 10.1016/j.margeo.2015.02.010.

571 Harris, Daniel L., Jody M. Webster, Ana Vila-concejo, Stephanie Duce, and Javier X. Leon. 2023.
572 "Geomorphology Defining Multi-Scale Surface Roughness of a Coral Reef Using a High-
573 Resolution LiDAR Digital Elevation Model." *Geomorphology* 439(September 2022):108852. doi:
574 10.1016/j.geomorph.2023.108852.

575 Hughes, Terry P., James T. Kerry, Mariana Álvarez-Noriega, Jorge G. Álvarez-Romero, Kristen D.
576 Anderson, Andrew H. Baird, Russell C. Babcock, Maria Beger, David R. Bellwood, Ray
577 Berkelmans, Tom C. Bridge, Ian R. Butler, Maria Byrne, Neal E. Cantin, Steeve Comeau, Sean R.
578 Connolly, Graeme S. Cumming, Steven J. Dalton, Guillermo Diaz-Pulido, C. Mark Eakin, Will F.
579 Figueira, James P. Gilmour, Hugo Harrison, Scott F. Heron, Andrew S. Hoey, Jean Paul A. Hobbs,
580 mia O. Hoogenboom, Emma V Kennedy, Chao Yang Kuo, Janice M. Lough, ryan J. Lowe, Gang
581 Liu, Malcolm T. McCulloch, Hamish A. Malcolm, michael J. McWilliam, John M. Pandolfi, rachel
582 J. Pears, morgan S. Pratchett, Verena Schoepf, Tristan Simpson, William J. Skirving, Brigitte
583 Sommer, Gergely Torda, David R. Wachenfeld, Bette L. Willis, and Shaun K. Wilson. 2017.
584 "Global Warming and Recurrent Mass Bleaching of Corals." *Nature* 543(7645):373–77. doi:
585 10.1038/nature21707.

586 Hughes, Terry P., James T. Kerry, Andrew H. Baird, Sean R. Connolly, Andreas Dietzel, C. Mark Eakin,
587 Scott F. Heron, Andrew S. Hoey, Mia O. Hoogenboom, Gang Liu, Michael J. McWilliam, Rachel J.
588 Pears, Morgan S. Pratchett, William J. Skirving, Jessica S. Stella, and Gergely Torda. 2018.
589 "Global Warming Transforms Coral Reef Assemblages." *Nature* 556(7702):492–96. doi:
590 10.1038/s41586-018-0041-2.

591 Jell, John S., and Gregory E. Webb. 2012. "Geology of Heron Island and Adjacent Reefs, Great Barrier
592 Reef, Australia." *Episodes* 35(1):110–19. doi: 10.18814/epiiugs/2012/v35i1/010.

593 Kench, Paul S., Edward P. Beetham, Tracey Turner, Kyle M. Morgan, Susan D. Owen, and Roger. F.
594 McLean. 2022. “Sustained Coral Reef Growth in the Critical Wave Dissipation Zone of a
595 Maldivian Atoll.” *Communications Earth & Environment* 3(1):1–12. doi: 10.1038/s43247-021-
596 00338-w.

597 Kench, Paul S., Murray R. Ford, and Susan D. Owen. 2019. “Patterns of Island Change and Persistence
598 Offer Alternate Adaptation Pathways for Atoll Nations.” *Nature Communications* 9(1). doi:
599 10.1038/s41467-018-02954-1.

600 Knutson, Thomas R., Joseph J. Sirutis, Ming Zhao, Robert E. Tuleya, Morris Bender, Gabriel A. Vecchi,
601 Gabriele Villarini, and Daniel Chavas. 2015. “Global Projections of Intense Tropical Cyclone
602 Activity for the Late Twenty-First Century from Dynamical Downscaling of CMIP5/RCP4.5
603 Scenarios.” *Journal of Climate* 28(18):7203–24. doi: 10.1175/JCLI-D-15-0129.1.

604 Lashley, Christopher H., Dano Roelvink, Ap van Dongeren, Mark L. Buckley, and Ryan J. Lowe. 2018.
605 “Nonhydrostatic and Surfbeat Model Predictions of Extreme Wave Run-up in Fringing Reef
606 Environments.” *Coastal Engineering* 137(October 2017):11–27. doi:
607 10.1016/j.coastaleng.2018.03.007.

608 Lowe, R. J., J. L. Falter, M. D. Bandet, G. Pawlak, M. J. Atkinson, S. G. Monismith, and J. R. Koseff.
609 2005. “Spectral Wave Dissipation over a Barrier Reef.” *J. Geophys. Res* 110:4001. doi:
610 10.1029/2004JC002711.

611 Madin, Joshua S., and Sean R. Connolly. 2006. “Ecological Consequences of Major Hydrodynamic
612 Disturbances on Coral Reefs.” *Nature* 444(7118):477–80. doi: 10.1038/nature05328.

613 Massel, S. R., and M. R. Gourlay. 2000. “On the Modelling of Wave Breaking and Set-up on Coral
614 Reefs.” *Coastal Engineering* 39(1):1–27. doi: 10.1016/S0378-3839(99)00052-6.

615 Masselink, Gerd, Eddie Beetham, and Paul Kench. 2020. “Coral Reef Islands Can Accrete Vertically in
616 Response to Sea Level Rise.” *Sci. Adv* 6(June):3656–66.

Meucci, Alberto, Ian R. Young, Mark Hemer, Ebru Kirezci, and Roshanka Ranasinghe. 2020. "Projected 21st Century Changes in Extreme Wind-Wave Events." *Science Advances* 6(24):7295–7305. doi: 10.1126/sciadv.aaz7295.

Monismith, Stephen G., Liv M.M. Herdman, Soeren Ahmerkamp, and James L. Hench. 2013. "Wave Transformation and Wave-Driven Flow across a Steep Coral Reef." *Journal of Physical Oceanography* 43(7):1356–79. doi: 10.1175/JPO-D-12-0164.1.

Monismith, Stephen G., Liv M. M. Herdman, Soeren Ahmerkamp, and James L. Hench. 2013. "Wave Transformation and Wave-Driven Flow across a Steep Coral Reef." *Journal of Physical Oceanography* 43(7):1356–79. doi: 10.1175/JPO-D-12-0164.1.

Monismith, Stephen G., Justin S. Rogers, David Koweek, and Robert B. Dunbar. 2015. "Frictional Wave Dissipation on a Remarkably Rough Reef." *Geophysical Research Letters* 42(10):4063–71. doi: 10.1002/2015GL063804.

Montaggioni, Lucien F. 2005. "History of Indo-Pacific Coral Reef Systems since the Last Glaciation: Development Patterns and Controlling Factors." *Earth-Science Reviews* 71(1–2):1–75. doi: 10.1016/j.earscirev.2005.01.002.

Munk, Walter H., and Martson C. Sargent. 1948. "Adjustment of Bikini Atoll to Ocean Waves." *Transactions, American Geophysical Union* 29(6):855. doi: 10.1029/TR029i006p00855.

Osorio-Cano, Juan D., Juan C. Alcérreca-Huerta, Andrés F. Osorio, and Hocine Oumeraci. 2018. "CFD Modelling of Wave Damping over a Fringing Reef in the Colombian Caribbean." *Coral Reefs* 37(4):1093–1108. doi: 10.1007/s00338-018-1736-4.

Pepper, A., and M. L. Puotinen. 2009. "Gremo: A GIS-Based Generic Model for Estimating Relative Wave Exposure." *18th World IMACS Congress and MODSIM 2009 - International Congress on Modelling and Simulation: Interfacing Modelling and Simulation with Mathematical and Computational Sciences, Proceedings* 1964–70.

641 Péquignet, A. C., J. M. Becker, M. A. Merrifield, and S. J. Boc. 2011. “The Dissipation of Wind Wave
642 Energy across a Fringing Reef at Ipan, Guam.” *Coral Reefs* 30(SUPPL. 1):71–82. doi:
643 10.1007/s00338-011-0719-5.

644 Péquignet, Anne-Christine N., Janet M. Becker, and Mark A. Merrifield. 2014. “Energy Transfer
645 between Wind Waves and Low-Frequency Oscillations on a Fringing Reef, Ipan, Guam.” *Journal*
646 *of Geophysical Research: Oceans* 119(10):6709–24. doi: 10.1002/2014JC010179.

647 Perry, Chris T., Lorenzo Alvarez-Filip, Nicholas A. J. Graham, Peter J. Mumby, Shaun K. Wilson, Paul S.
648 Kench, Derek P. Manzello, Kyle M. Morgan, Aimee B. A. Slangen, Damian P. Thomson, Fraser
649 Januchowski-Hartley, Scott G. Smithers, Robert S. Steneck, Renee Carlton, Evan N. Edinger, Ian
650 C. Enochs, Nuria Estrada-Saldívar, Michael D. E. Haywood, Graham Kolodziej, Gary N. Murphy,
651 Esmeralda Pérez-Cervantes, Adam Suchley, Lauren Valentino, Robert Boenish, Margaret
652 Wilson, and Chancey MacDonald. 2018. “Loss of Coral Reef Growth Capacity to Track Future
653 Increases in Sea Level.” *Nature* 558(7710):396–400. doi: 10.1038/s41586-018-0194-z.

654 Quataert, Ellen, Curt Storlazzi, Ap van Dongeren, and Robert McCall. 2020. “The Importance of
655 Explicitly Modelling Sea-Swell Waves for Runup on Reef-Lined Coasts.” *Coastal Engineering*
656 160(April):103704. doi: 10.1016/j.coastaleng.2020.103704.

657 Quataert, Ellen, Curt Storlazzi, Arnold Van Rooijen, Olivia Cheriton, and Ap Van Dongeren. 2015a.
658 “The Influence of Coral Reefs and Climate Change on Wave-Driven Flooding of Tropical
659 Coastlines.” *Geophysical Research Letters* 42(15):6407–15. doi: 10.1002/2015GL064861.

660 Quataert, Ellen, Curt Storlazzi, Arnold Van Rooijen, Olivia Cheriton, and Ap Van Dongeren. 2015b.
661 “The Influence of Coral Reefs and Climate Change on Wave-Driven Flooding of Tropical
662 Coastlines.” *Geophysical Research Letters* 42(15):6407–15. doi: 10.1002/2015GL064861.

663 Reguero, Borja G., Iñigo J. Losada, and Fernando J. Méndez. 2019. “A Recent Increase in Global Wave
664 Power as a Consequence of Oceanic Warming.” *Nature Communications* 10(1):1–14. doi:

10.1038/s41467-018-08066-0.

Roelvink, Dano, A. Reniers, Ap van Dongeren, J. S. M. van Thiel de Vries, J. Lescinski, and R. T. McCall. 2015. *XBeach Model Description and Manual*.

Rogers, Justin S., Stephen G. Monismith, Falk Feddersen, and Curt D. Storlazzi. 2013. "Hydrodynamics of Spur and Groove Formations on a Coral Reef." *Journal of Geophysical Research: Oceans* 118(6):3059–73. doi: 10.1002/jgrc.20225.

Rogers, Justin S., Stephen G. Monismith, Oliver B. Fringer, David A. Koweek, and Robert B. Dunbar. 2017. "A Coupled Wave-Hydrodynamic Model of an Atoll with High Friction: Mechanisms for Flow, Connectivity, and Ecological Implications." *Ocean Modelling* 110. doi: 10.1016/j.ocemod.2016.12.012.

Rogers, Justin S., Stephen G. Monismith, David A. Koweek, and Robert B. Dunbar. 2016. "Wave Dynamics of a Pacific Atoll with High Frictional Effects." *Journal of Geophysical Research: Oceans* 121(1):350–67. doi: 10.1002/2015JC011170.

Sanborn, Kelsey L., Jody M. Webster, Gregory E. Webb, Juan Carlos Braga, Marc Humblet, Luke Nothdurft, Madhavi A. Patterson, Belinda Dechnik, Susan Warner, Trevor Graham, Richard J. Murphy, Yusuke Yokoyama, Stephen P. Obrochta, Jian xin Zhao, and Marcos Salas-Saavedra. 2020. "A New Model of Holocene Reef Initiation and Growth in Response to Sea-Level Rise on the Southern Great Barrier Reef." *Sedimentary Geology* 397:105556. doi: 10.1016/j.sedgeo.2019.105556.

Saunders, Megan I., Simon Albert, Chris M. Roelfsema, Javier X. Leon, Colin D. Woodroffe, Stuart R. Phinn, and Peter J. Mumby. 2016. "Tectonic Subsidence Provides Insight into Possible Coral Reef Futures under Rapid Sea-Level Rise." *Coral Reefs* 35(1):155–67. doi: 10.1007/s00338-015-1365-0.

Sheppard, Charles. 1981. "The Groove and Spur Structures of Chagos Atolls and Their Coral

689 Zonation." *Estuarine, Coastal and Shelf Science* 12(5):549–60. doi: 10.1016/S0302-
690 3524(81)80081-3.

691 Sheppard, Charles, David J. Dixon, Michael Gourlay, Anne Sheppard, and Rolph Payet. 2005. "Coral
692 Mortality Increases Wave Energy Reaching Shores Protected by Reef Flats: Examples from the
693 Seychelles." *Estuarine, Coastal and Shelf Science* 64(2–3):223–34. doi:
694 10.1016/j.ecss.2005.02.016.

695 Shinn, Eugene. 1963. "Spur and Groove Formation on the Florida Reef Tract." *SEPM Journal of*
696 *Sedimentary Research* Vol. 33(2):291–303. doi: 10.1306/74d70e34-2b21-11d7-
697 8648000102c1865d.

698 Shukla, P. R., J. Skea, R. Slade, R. van Diemen, E. Haughey, J. Malley, M. Pathak, and J. Portugal
699 Pereira. 2019. *IPCC, 2019: Technical Summary*.

700 Shukla, P. R., J. Skea, R. Slade, R. van Diemen, E. Haughey, J. Malley, M. Pathak, and J. Portugal
701 Pereira. 2019. *IPCC, 2019: Technical Summary*.

702 da Silva, Renan F., Curt D. Storlazzi, Justin S. Rogers, Johan Reyns, and Robert McCall. 2020.
703 "Modelling Three-Dimensional Flow over Spur-and-Groove Morphology." *Coral Reefs*. doi:
704 10.1007/s00338-020-02011-8.

705 Smith, Courtney, Tristan Salles, and Ana Vila-Concejo. 2022. "Offshore Wave Climate of the Great
706 Barrier Reef." *In Review* (0123456789). doi: 10.1007/s00338-023-02377-5.

707 Smith, Courtney, Ana Vila-Concejo, and T. B. Salles. 2020. "RADWave: Python Code for Ocean
708 Surface Wave Analysis by Satellite Radar Altimeter." *Journal of Open Source Software* 1(5):46.
709 doi: https://doi.org/10.21105/joss.02083.

710 Smyth, C., and Alex A. Hay. 2002. "Wave Friction Factors in Nearshore Sands." *Journal of Physical*
711 *Oceanography* 32(12):3490–98. doi: 10.1175/1520-0485(2002)032<3490:WFFINS>2.0.CO;2.

712 Sous, Damien, Samantha Maticka, Samuel Meulé, and Frédéric Bouchette. 2022. “Bottom Drag
713 Coefficient on a Shallow Barrier Reef.” *Geophysical Research Letters* 1–12. doi:
714 10.1029/2021gl097628.

715 Storlazzi, C. D., E. K. Brown, M. E. Field, K. Rodgers, and P. L. Jokiel. 2005. “A Model for Wave Control
716 on Coral Breakage and Species Distribution in the Hawaiian Islands.” *Coral Reefs* 24(1):43–55.
717 doi: 10.1007/s00338-004-0430-x.

718 Storlazzi, Curt D., Edwin P. L. Elias, and Paul Berkowitz. 2015. “Many Atolls May Be Uninhabitable
719 Within Decades Due to Climate Change.” *Scientific Reports* 5(1):1–9. doi: 10.1038/srep14546.

720 Talavera, Lara, Ana Vila-Concejo, Jody M. Webster, Courtney Smith, Stephanie Duce, Thomas E.
721 Fellowes, Tristan Salles, Daniel Harris, Jon Hill, Will Figueira, and Jörg Hacker. 2021.
722 “Morphodynamic Controls for Growth and Evolution of a Rubble Coral Island.” *Remote Sensing*
723 13(8):1–23. doi: 10.3390/rs13081582.

724 Yao, Yu, Yicheng Liu, Long Chen, Zhengzhi Deng, and Changbo Jiang. 2020. “Study on the Wave-
725 Driven Current around the Surf Zone over Fringing Reefs.” *Ocean Engineering* 198. doi:
726 10.1016/j.oceaneng.2020.106968.

727 Young, I. R. 1992. “The Determination of Spectral Parameters from Significant Wave Height and Peak
728 Period.” *Ocean Engineering* 19(5):497–508. doi: 10.1016/0029-8018(92)90008-R.

729